Comparison study of physicochemical and biopharmaceutics properties of hydrophobic drugs ground by two dry milling processes.

M. Dandignac, Suenia de Paiva Lacerda, Alain Chamayou, Laurence Galet

Comparison study of physicochemical and biopharmaceutics properties of hydrophobic drugs ground by two dry milling processes

M. Dandignac, S. P. Lacerda, A. Chamayou and L. Galet

Université de Toulouse, IMT Mines Albi, UMR CNRS 5302, Centre RAPSODEE, Albi Cedex, France

ABSTRACT

This study focuses on the dry milling of biopharmaceutical classification system (BCS) class II molecules. These molecules have a limited bioavailability because of their low aqueous solubility, poor water wettability and low dissolution rate. In order to improve these properties, indomethacin (IND) and niflumic acid (NIF) were milled using two different types of equipment: Pulverisette 0® and CryoMill®. Milled samples were characterized and compared to commercial molecules. IND shows a modified solid state, like surface crystallinity reduction and an increase in water vapor adsorption from to 2- up to 5-fold due to milling processes. The obtained solubility data resulted in an improvement in solubility up to 1.2-fold and an increase in initial dissolution kinetics: 2% of dissolved drug for original crystals against 25% for milled samples. For NIF no crystallinity reduction, no change of surface properties and no solubility improvement after milling were noticed. In addition, milled particles seemed more agglomerated resulting in no changes in dissolution rate compared to the original drug. IND solubility and dissolution enhancement can be attributed to the modification of surface area, drug crystallinity reduction, and water sorption increase due to specific behavior related to the drug crystal disorder induced by milling process.

1. Introduction

In industrial fields, the design of New Chemical Entities (NCE) through combinatorial chemistry has led to the development of drug candidates with greater lipophilicity, high molecular weight, and poor water solubility. These physical, chemical, and intrinsic drug properties are considered as the major obstacle that has prevented the commercialization of many new promising drugs. However, majority pharmaceutical development failure has been attributed to poor water solubility of the drug.

Nowadays, 90% of pharmaceutical solid dosage form contains hydrophobic substances (Al-Obaidi et al. 2013). Many of these compounds are classified as class II and IV in the biopharmaceutical classification system (BCS) (Amidon et al. 1995). The compounds of this molecules class are characterized by poor solubility.

Issues of drugs poor water solubility provide limitation on dissolution rate and reduction on oral bioavailability resulting in suboptimal drug delivery. Early-stage pharmaceutical development is the critical step to the development of this kind of pharmaceutical products. To overcome solubility issues, powder technology provides new innovative solutions for original as well as generic applications in a wide variety of industries including pharmaceuticals.

There are many strategies to overcome low solubility or low dissolution rate of hydrophobic drugs. Different approaches include systems that emphasize physical: size reduction (Chamarthy and Pinal 2008; Branham et al. 2012; Borba et al. 2016), chemical modifications: amorphization (Chaudhari and Dugar 2017) or new solid forms such as carrier systems like solid dispersion (Chikhalia et al. 2006; Chaudhary et al. 2012). Other different approaches are known such as pH adjustment (Columbano et al. 2003; Saravanan et al. 2021), salt formation (Da Silva et al. 2020), the use of co-solvents (De Gusseme et al. 2008), complexation (de Paiva Lacerda et al. 2015; Dedroog et al. 2019), addition of surfactants (Dujardin et al. 2013; Einfalt et al. 2013), formulation as emulsion or other lipid based systems or entrapment in liposomes (Feng et al. 2008; El-Badry et al. 2009).

Among the conventional methods for bioavailability improvement, size reduction, in the micrometer or nanometer scales, is an important and widely used operation in many pharmaceutical applications to optimize active drug physicochemical properties and consequently the performance and the manufacturing of pharmaceuticals dosage forms. Particle size reduction methods can be divided into two main categories, bottom-up and top-down techniques. Top down features dry milling in particular, which is often used to reduce the particle size in the absence of water or any organic solvent. In addition, this method is easy to handle, reproducible and represents a low-cost method to improve solubility and/or dissolution kinetics (Fix and Steffens 2004) by multiple mechanisms as size reduction (Friedrich et al. 2005), crystal modification, amorphization (Garg et al. 2009) up to powder surface modification (Gotor et al. 2013). Different types of ball milling equipment were tested in this work. Their size reduction mechanisms are based on impaction and compression (Guo et al. 2013; Hadjittofis et al. 2018). The balls impact and the compression phenomenon from their movement can affect the potential of particle size reduction and create aggregate (Han et al. 2011; Hagbani and Nazzal 2017). In addition, ratio between the material and the ball can also have an impact on milling intensity (Humayun et al. 2016; Hussain et al. 2018).

Dry ball milling, as a micronization technique, is well known and supported by the literature (Jójárt et al. 2012; Jermain et al.

CONTACT S. P. Lacerda suenia.depaivalacerda@mines-albi.fr Université de Toulouse, IMT Mines Albi, UMR CNRS 5302, Centre RAPSODEE, Campus Jarlard, Albi Cedex 09 F-81013, France

2018). Moreover, this milling process is adapted to hydrophobic drugs to improve their physicochemical properties (Junyaprasert and Morakul 2015) and increase drug solubility and/or dissolution kinetics (Kacso et al. 2012), as represented in the Noyes–Whitney equation (Kho et al. 2014). Therefore, the purpose of the present work is (i) to determine the physicochemical properties of two different BCS Class II (indomethacin (IND) and niflumic acid (NIF)) and (ii) to increase their solubility and improve their dissolution kinetics considering the effect of ball dry milling through two different types of equipment (Pulverisette 0® and CryoMill®).

In the first part of the work, model drugs were selected based on their BCS classification (i.e. poorly water-soluble drugs), assay method described in pharmacopeia, easy availability, and low handling risks. In the second part, ground powders produced by dry milling were characterized according to their physicochemical properties through thermal analysis, particle size distribution (PSD) particles morphology, surface changing, powder crystallinity, and finally solubility and dissolution kinetics.

2. Materials and methods

2.1. Materials

Active pharmaceutical ingredients (APIs), IND (γ-form), and NIF were provided from Tokyo Chemical Industry (TCI Europe, Zwijndrecht, Belgium). Both APIs have 98% of purity. For high-performance liquid chromatography (HPLC) analysis, acetonitrile (ACN), acetic acid HPLC grade were purchased from VWR (Fontenay-sous-Bois, France), distilled and purified water were obtained by the purification system Milli-Q (Classic Purelab DI, MK2, Elga, High Wycombe, UK).

2.2. Grinding process

2.2.1. Preparation of ground drug

Dry grinding process was performed using Pulverisette 0® (Fritsch, Idar-Oberstein, Germany) and CryoMill® (Retsch, Haan, Germany). For each grinding experiment, one stainless-steel ball is placed in the stainless-steel jar. The milling process parameters, of both types of grinding equipment, are described in Table 1. Sample nomenclature and process conditions of each sample are detailed in Table 2. The same process parameters were applied to IND and NIF.

2.2.2. Yield calculation

Actual yields were calculated as the percentage by mass of the powder recovered after grinding in relation to the total initial amount of drug used for grinding.

2.3. Physicochemical characterization

2.3.1. Drug content

The quantification of the IND and NIF, obtained by grinding, was determined by solubilization of approximately 5 mg of powder in 50 g ACN/water (50/50, w/w) to obtain a final concentration of 0.1 mg g^{-1}. Each sample was analyzed in duplicate ($n = 2$). API assay was performed by UHPLC (Infinity II 1290, Agilent, Massy, France) equipped with a UV-Vis detector. A reverse phase HPLC method was used for the quantification using a method according to the European Pharmacopeia. The mobile phase was ACN/acetic acid 0.01%, (50/50 v/v), the flow rate was 1 mL/min, the volume of injection was 20 µL and wavelength was fixed at 318 nm. A Poroshell® 120 EC-C18 column 2.7 µm (3 × 100 mm, Agilent, Massy, France) was used. The retention times were at 1.5 and 1.2 min for IND and NIF, respectively. The results were expressed as the percentage of the mean of the peak responses of ground APIs related to the mean of the peak responses of the raw material, which was considered as 100%.

2.3.2. Particle size analysis

The PSDs of samples were determined by laser diffraction particle size analyzer, a MasterSizer 3000 laser granulometer (Malvern Instruments, Malvern, UK). Samples were dispersed in water without ultrasonication.

2.3.3. Scanning electron microscopy (SEM) analysis

The surface morphology of samples was observed with a tabletop scanning electron microscope (MT-3000, Hitachi, Tokyo, Japan) operated at an excitation voltage of 15 kV in SE mode. A double-sided adhesive tape was used to fix the powder sample on an SEM stub before analysis.

2.3.4. X-ray powder diffraction (XRPD) analysis

Powder diffractograms were obtained using an X-ray diffractometer (X'Pert Panalytical, Philips, Cambridge, MA) with CuKα radiation at a scanning rate of 1.228 min^{-1} from 5° to 50° with a measurement step of 0.017°, applying 45 kV at 40 mA to observe the crystallinity of the sample.

Table 1. Grinding parameters.

Milling equipment	Ball diameter (cm)/mass (g)	API mass (g)	Milling time (min)	Frequency (Hz)	Amplitude (mm)
Pulverisette 0®	5/500	1, 2, and 3	20	–	1.5 and 1.8
CryoMill®	1/60	2	2.5 and 5	12.5 and 25	–

Table 2. Sample nomenclature.

Milling equipment	Sample name	Amplitude (mm)	Frequency (Hz)	API mass (g)	Milling time (min)
P0	P1	1.5	–	1	20
	P2	1.5	–	2	20
	P3	1.5	–	3	20
	P4	1.8	–	1	20
	P5	1.8	–	2	20
	P6	1.8	–	3	20
CM	CM1	–	12.5	2	2.5
	CM2	–	12.5	2	5
	CM3	–	25	2	2.5
	CM4	–	25	2	5

2.3.5. Differential scanning calorimetry

Differential scanning calorimetry (DSC) measurements were carried out using a DSC-Q200 thermal analyzer (TA Instrument, Guyancourt, France) in a temperature range of 20–210 °C (heating rate 5 °C.min^{-1}) under nitrogen gas with a flow rate of 50 mL min^{-1}. Samples of raw material and milled powder (2.8–5.5 mg) were placed in a hermetically closed aluminum pan. The heat of fusion (ΔH_F) and melting temperature (T_m) were calculated using the DSC software (Platinum®). The residual crystallinity (χ_c) was calculated using Equation (1), taking into account the melting enthalpy of 100% crystalline sample (raw material) and ground one (Kumar et al. 2018).

$$\chi_c(\%) = \frac{\Delta H_{m(\text{grinded sample})}}{\Delta H_{m(100\% \text{ crystallin})}} \times 100 \quad (1)$$

2.3.6. Fourier-transform infrared (FTIR) spectroscopy

FTIR spectra were recorded on a Thermo Scientific Nicolet™ iS50 spectrometer, using Omnic® software to analyze the data. The samples were placed on the diamond window. The data were recorded in ATR mode in a scan range of 4000–400 cm^{-1} with a resolution of 4 cm^{-1}.

2.3.7. Dynamic vapor sorption (DVS)

The dynamic vapor sorption measurements were carried out on the DVS apparatus of the SMS (Surface Measurement Systems) (Allentown, PA). All experiments were performed at 25 °C. Dry nitrogen is blown through the probe for 60 min. The relative pressure of the probe is controlled using a computer program that sets the appropriate flow rate on the wet side (100% relative pressure of the probe) and the dry side (dry nitrogen). Fifty to 100 mg was placed into the pods. Measurements were recorded on a scale from 0 to 95% relative humidity (RH) with a measurement step of 10% RH. The final step was set at 95% RH. Two measurement cycles were conducted.

2.3.8. Solubility measurement

Solubility of samples was determined using a method previously described in the literature (Borba et al. 2016), by equilibrating a drug excess in 30 g of phosphate buffer pH 7.2 at 37 ± 0.5 °C in a temperature-controlled bath up to 48 h (equilibrium). The flasks were sealed and shaken for the duration of the tests and concentrations were determined after filtration (0.22 µm, VWR, Fontenay-sous-Bois, France). The sample solutions were analyzed using the same assay method as described for drug content determination. Each experiment was carried out in quadruplicate.

The relative solubility (RS) was calculated using Equation (2) taking into account the solubility value of raw API and ground sample.

$$\text{RS } (\%) = \frac{\text{solubility value}_{\text{sample}}}{\text{solubility value}_{\text{raw API}}} \times 100 \quad (2)$$

2.3.9. Dissolution kinetics measurement

The apparent dissolution ($n = 3$) tests were carried out using dissolution method a USP II dissolution apparatus (AT Xtend, SOTAX, Aesch, Switzerland). Paddle speeds were set at 100 rpm with 500 mL of phosphate buffer pH 7.2 at 37 ± 0.5 °C; to ensure sink conditions, approximately 51 mg for IND and 140 mg for NIF (taking into account drug content). Each drug sample was placed into a hard-shell capsule and fixed to the bottom of the dissolution vessel by stain steel sinkers. At appropriate time intervals: 5, 10, 15, 30, 45, and 60 min, 2 mL of samples were withdrawn and filtered through a 0.22 µm filter (VWR, Fontenay-sous-Bois, France). API dissolved assay was analyzed using UHPLC method as described in the drug content determination part.

The dissolved drug (DD) as a percentage was calculated using Equation (3) taking into account the theoretical concentration value of raw API and the concentration of ground sample at each time point.

$$\text{DD } (\%)(t) = \frac{\text{Concentration}_{\text{sample (t)}}}{\text{Concentration}_{\text{raw API}}} \times 100 \quad (3)$$

3. Results and discussion

3.1. Grinding analysis on process yield and drug purity

3.1.1. Purity and yield

The grinding process has no impact on API purity. For all ground powders, the purity was above 93%. Yield (final product) of 81–97% was obtained after grinding (Table 3).

3.1.2. Particle size distribution and powder morphology

The PSD provides information related to product size reduction and subsequent milling performance. Upon reviewing results of measurement data, particle number and volume size distributions are plotted in Figure 1. It could be observed on the number % PSD that ground products show clearly smaller sizes than raw material. Besides, a slight decrease of particle volume size distributions were observed. These results are supported by the finer and the more agglomerate powders produced after milling, as shown in Figure 2(1,2). For clarity, the characteristic sizes of the product particle, the mean size based on volume and the mean size based on surface/volume (D [4,3] and D [3,2]) are summarized in Table 4.

For both APIs ground using the Pulverisette 0®, it was observed that a higher API mass inside the apparatus is more likely to achieve a higher degree of size reduction. For IND,

Table 3. Yield and purity results.

	IND			NIF		
Milling equipment	Sample name	Yield (%)	Purity (%)	Sample name	Yield (%)	Purity (%)
P0	INDP1	84	95	NIFP1	80	90
	INDP2	87	93	NIFP2	88	95
	INDP3	90	97	NIFP3	90	98
	INDP4	81	96	NIFP4	81	100
	INDP5	88	93	NIFP5	87	99
	INDP6	89	95	NIFP6	90	100
CM	INDCM1	88	97	NIFCM1	94	97
	INDCM2	89	94	NIFCM2	96	100
	INDCM3	90	97	NIFCM3	97	100
	INDCM4	89	95	NIFCM4	97	93

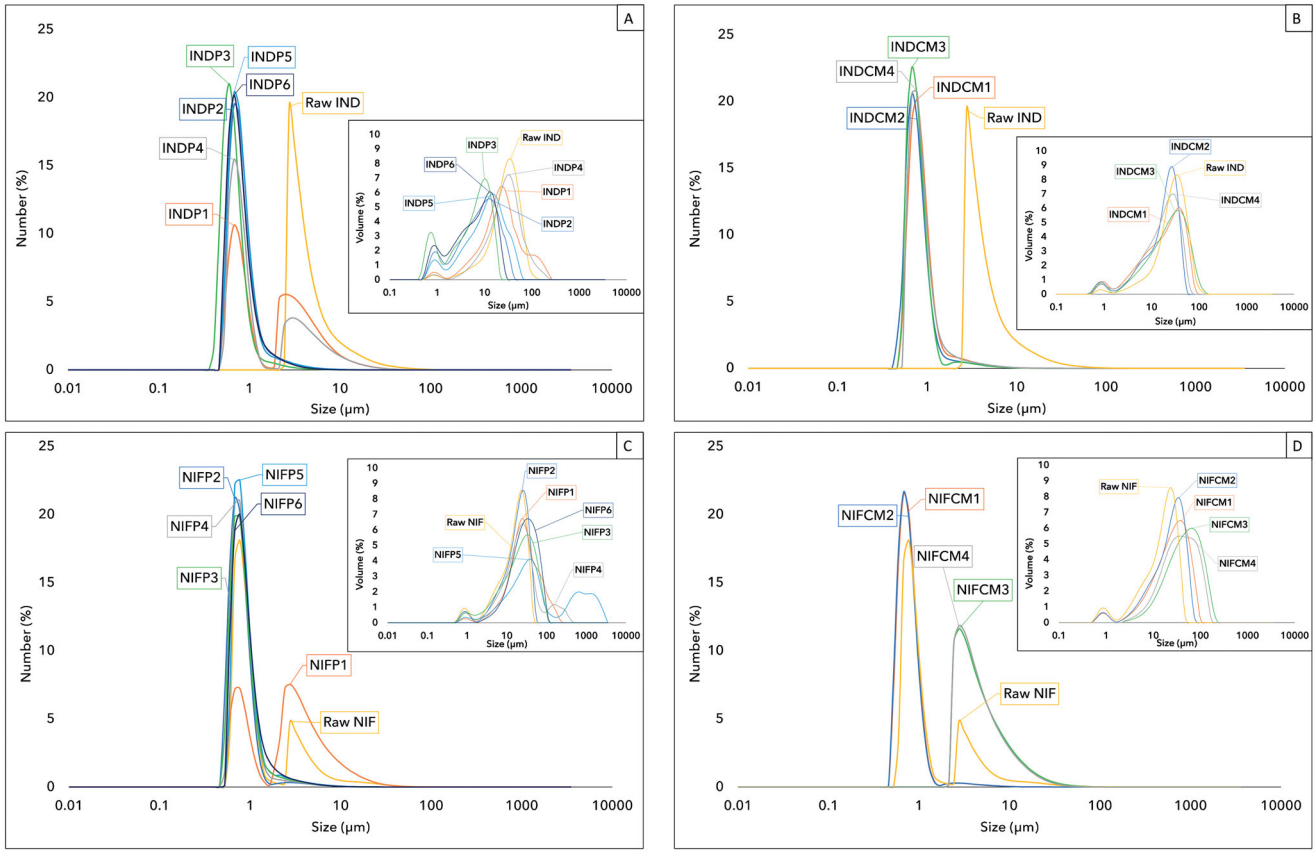

Figure 1. Particle size distribution. (A) IND ground with Pulverisette 0®, (B) IND ground with CryoMill®, (C) NIF ground with Pulverisette 0®, and (D) NIF ground with CryoMill®.

particle reduction observed was between 2 and 6 folds and for NIF it was between 2- and 4-fold. Concerning the CryoMill®, ground IND showed a particle size decrease around two folds and NIF particle size reduction was next to threefold, regardless of the grinding time and frequency used.

Figure 2(1,2) qualitatively reveals, by SEM, ground particles morphology. Raw IND particle shape changed after milling on very small columnar crystals. On the other hand, particle morphology of starting NIF powder is similar to the ground one. However, smaller crystals are obtained. Nevertheless, for both APIs, grinding process had an impact on the crystals breakage and powder agglomeration state, which supports the results concerning the particle size.

3.2. Milling impact on crystalline APIs

The samples crystallinity evaluation was carried out by two complementary approaches: X-ray diffraction (XRD) and DSC, the combination of which allows a good understanding of crystal disorder (i.e. creation of amorphous regions and crystalline lattice defects; Kumar et al. 2022) induced by milling. XRD has shown useful insights related to diffraction method that give a great amount of valuable information concerning the crystal structure (Li et al. 2017), orientation and size (Ling et al. 2019) of ordered regions in materials (Loftsson and Brewster 2010) while DSC concerns thermal analysis which allows a more accurate determination of the melting enthalpy or the degree of crystallinity (Loh et al. 2015).

3.2.1. X-ray powder diffraction analysis

The crystalline character of APIs after milling is characterized by the presence of multiple Bragg peaks. For raw IND (see Figure 3(A,B)), Bragg peaks of γ-IND are in accordance with the reference data (Mallick et al. 2008). The most intense peaks were found at 2θ degrees of 10.2°, 11.7°, 16.7°, 19.6°, 20.5°, and 21.9°. However, after milling, a decrease of crystallinity was observed for both processes, characterized by a loss or intensity decrease of distinct peaks in the diffraction pattern (Fix and Steffens 2004; Mallick et al. 2013) such as 2θ of 19.6° and 21.9°. This behavior, can suggest the formation of amorphous regions or formation of crystals defects (Mallick et al. 2013) subjected to repeated collisions ball-powder-wall of bowl (Mártha et al. 2013), specially for INDP1, INDP4, INDCM3, and INDCM4 samples, where higher intensity decrease was observed. This trend seems to be related to higher energy available to break down the crystalline lattice of the drug, during milling used for low mass of added product inside the Pulverisette 0® bowl (Mennini et al. 2016) and also to higher milling intensity in CryoMill®. Concerning NIF, XRPD patterns represented in Figure 3(C,D) show the same characteristic Bragg peaks for all samples before and after the milling process. In addition, different process parameters do not lead to decrease of peak intensity. The most intense peaks were found at 2θ degrees of 8.2°, 12.8°, 16.2°, 23.2°, and 25.3°, which are in agreement with previous published results (Mir et al. 2018).

3.2.2. Differential scanning calorimetry

To further investigate and better understand crystal disorder, the different samples were also thermally characterized using DSC. Thermal analysis showed that raw and milled material for either drug does not exhibit a glass transition (Tg), indicating that there is no amorphous phase (Newman and Zografi 2014) upon milling, but does show an endothermic (melting like) event.

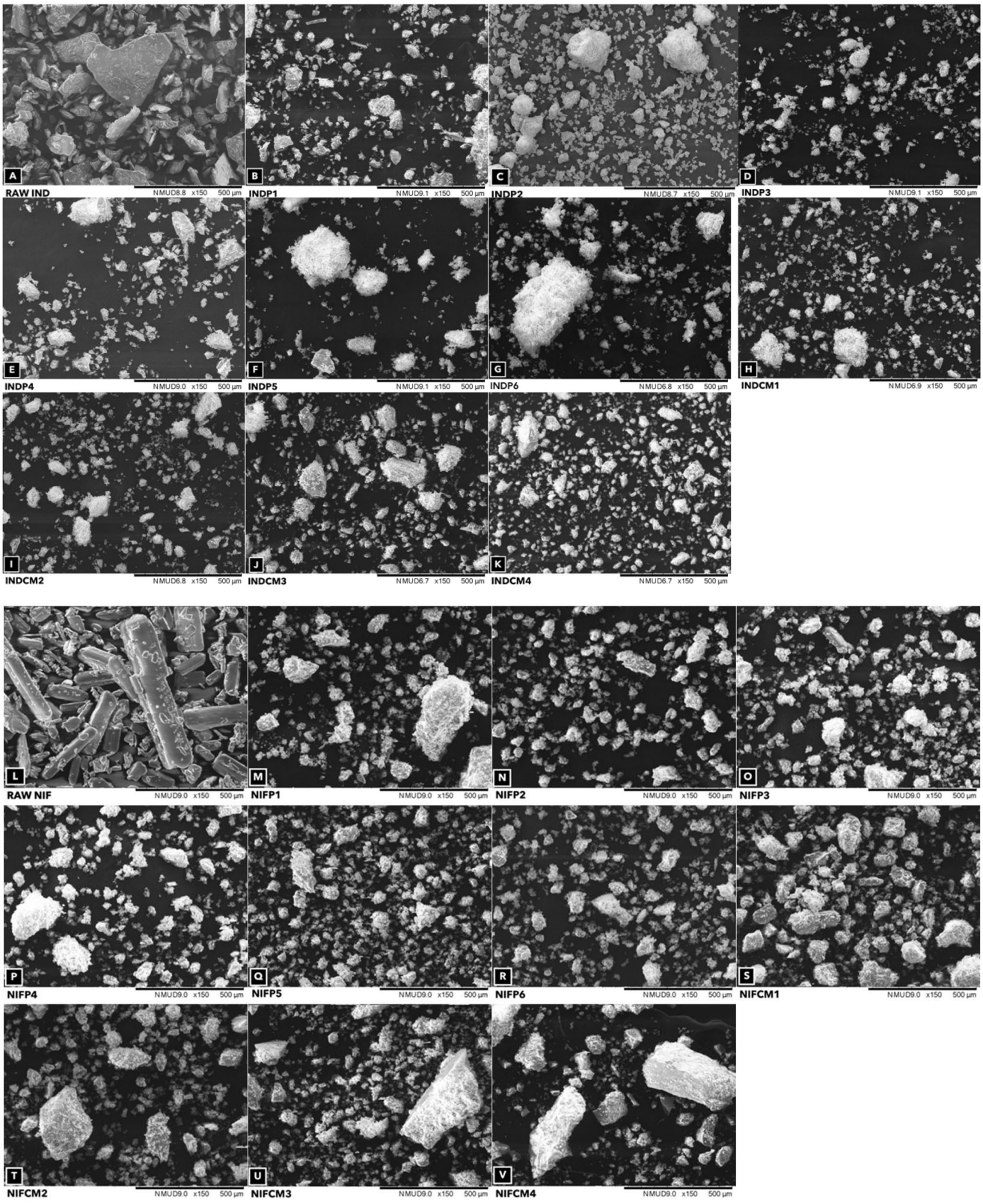

Figure 2. (1) SEM images of raw and ground IND. Raw IND (A); INDP1 (B); INDP2 (C); INDP3 (D); INDP4 (E); INDP5 (F); INDP6 (G); INDCM1(H); INDCM2 (I); INDCM3 (J); INDCM4 (K). (2) SEM images of raw and ground NIF. Raw NIF (L); NIFP1 (M); NIFP2 (N); NIFP3 (O); NIFP4 (P); NIFP5 (Q); NIFP6 (R); NIFCM1 (S); NIFCM2 (T); NIFCM3 (U); NIFCM4 (V).

For each sample, the IND DSC curve represented Figure 4(A,B), shows an endothermic peak of raw API at 160.3 °C which corresponds to γ-IND and is in accordance with the reference data (Mallick et al. 2008). The melting (onset) temperature and the heat of fusion for raw and ground samples are detailed in Table 5 as functions of different milling parameters. After milling, a slight depression of melting (onset) temperature (from 159.8 °C up to 157.6 °C), heat of fusion (from 111 J g^{-1} up to 104.2 J g^{-1}) and residual crystallinity (from 100% up to 94%) is observed (see Table 5). Residual cristallinity reduction was mainly noticed for INDP1,

Table 4. Particle size distribution of drug powders.

	IND				NIF			
Milling equipment	Sample name	Span	*D* [4,3] (μm)	*D* [3,2] (μm)	Sample name	Span	*D* [4,3] (μm)	*D* [3,2] (μm)
–	Raw IND	1.7	34.2	15.3	Raw NIF	10.1	87.1	35.8
P0	INDP1	1.3	38.1	16.7	NIFP1	1.6	40.0	19.7
	INDP2	0.7	11.0	4.3	NIFP2	0.7	21.5	9.2
	INDP3	0.7	7.2	2.7	NIFP3	0.8	18.8	7.6
	INDP4	1.1	37.7	16.3	NIFP4	0.8	43.3	10.5
	INDP5	0.8	15.5	5.8	NIFP5	0.8	27.8	9.1
	INDP6	0.9	8.6	3.3	NIFP6	0.9	29.1	9.2
CM	INDCM1	2.4	25.9	8.0	NIFCM1	0.7	32.2	11.7
	INDCM2	1.7	21.2	8.2	NIFCM2	0.6	27.6	10.6
	INDCM3	2.4	31.8	9.7	NIFCM3	2.1	61.3	30.9
	INDCM4	1.9	22.1	8.6	NIFCM4	2.1	50.1	25.5

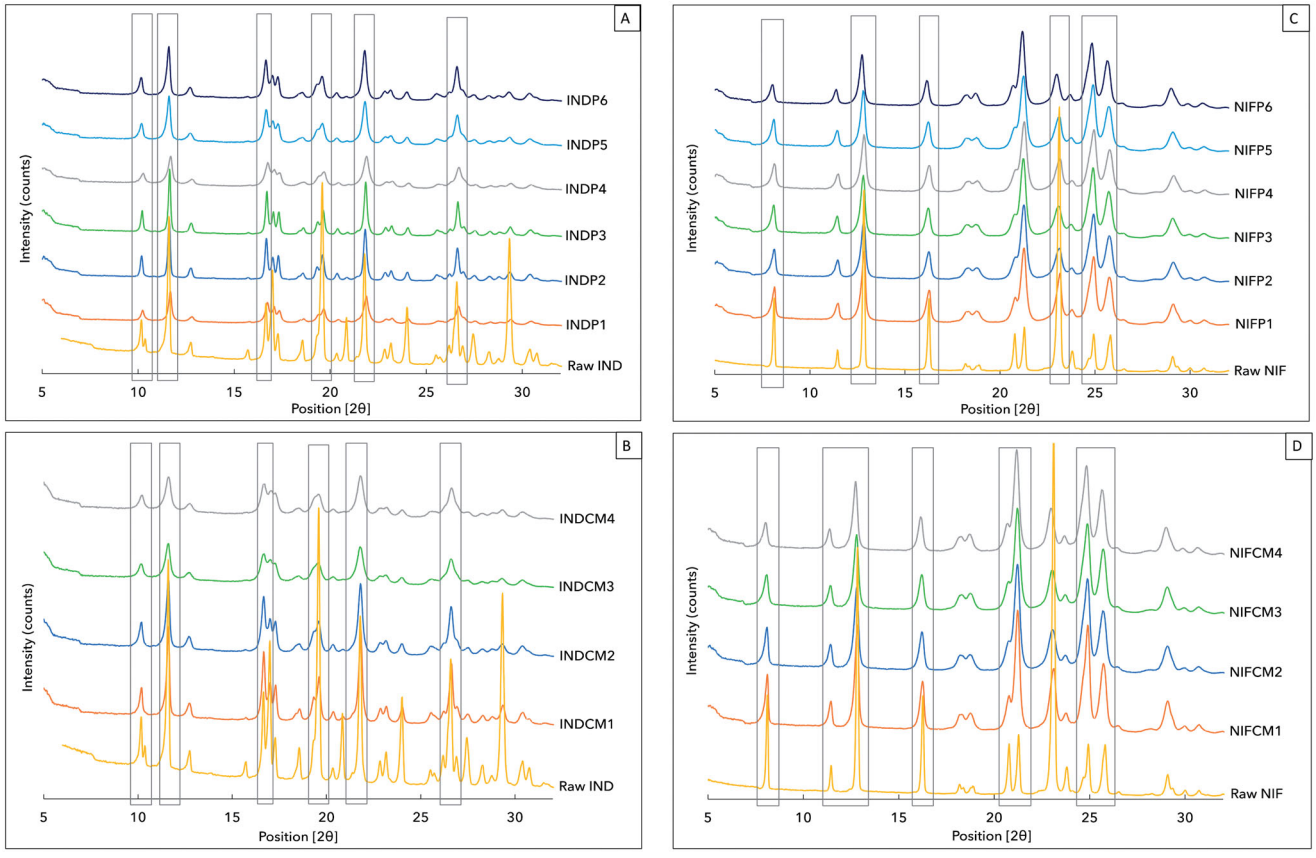

Figure 3. XRPD diffractogram. (A) IND ground with Pulverisette 0®, (B) IND ground with CryoMill®, (C) NIF ground with Pulverisette 0®, and (D) NIF ground with CryoMill®.

INDP4, INDCM3, and INDCM4 samples (bold values). These results can indicate a decrease in crystallinity (Noyes and Whitney 1897; Nugrahani and Jessica 2021) where the higher the energy applied during milling the greater the number of defects are formed (Patterson et al. 2007). The same tendency has been evidenced by the changes in the corresponding XRPD patterns analysis discussed previously. However, both approaches are not able to differentiate which property governs crystallinity loss: amorphous regions or formation of crystal defects (Mallick et al. 2013).

Raw NIF, has an endothermic peak at 203 °C (shown in Figure 3(C,D)), which is in accordance with previous work (Perissutti et al. 2017). According to Table 5, no changes in DSC thermal parameters were observed after milling in both types of equipment using different process parameters. In addition, after milling the residual crystallinity was maintained. As mentioned above for NIF, the XRPD results are also supported by the DSC analysis.

3.3. Grinding effect on powder chemical properties and powder surface characterization

3.3.1. Fourier-transform infrared spectroscopy characterization

FTIR was performed in order to detect APIs structural change (Phillips 1997; Qin et al. 2018; Sakher et al. 2018), after the milling process. In particular, the entire spectral range investigated is shown in Figure 5, whereas in a restricted range (600–1800 cm^{-1}) the principal absorption bands in the infrared spectra of unmilled and milled samples are observed. Based on the literature, γ-IND absorption bands are shown in Figure 5(A,B) (Saleki-Gerhardt et al. 1994). The most intense peaks at 1715 cm^{-1} and 1691 cm^{-1} (C=O stretching vibrations), 1615–1587 cm^{-1} and $\nu = 1480\ cm^{-1}$ (C=C stretching vibrations) are evidenced. The absorption peaks at 1307 cm^{-1} and 1240–1221 cm^{-1} correspond to C–O bond of acidic and ether groups, respectively. The peak at 1068 cm^{-1} can

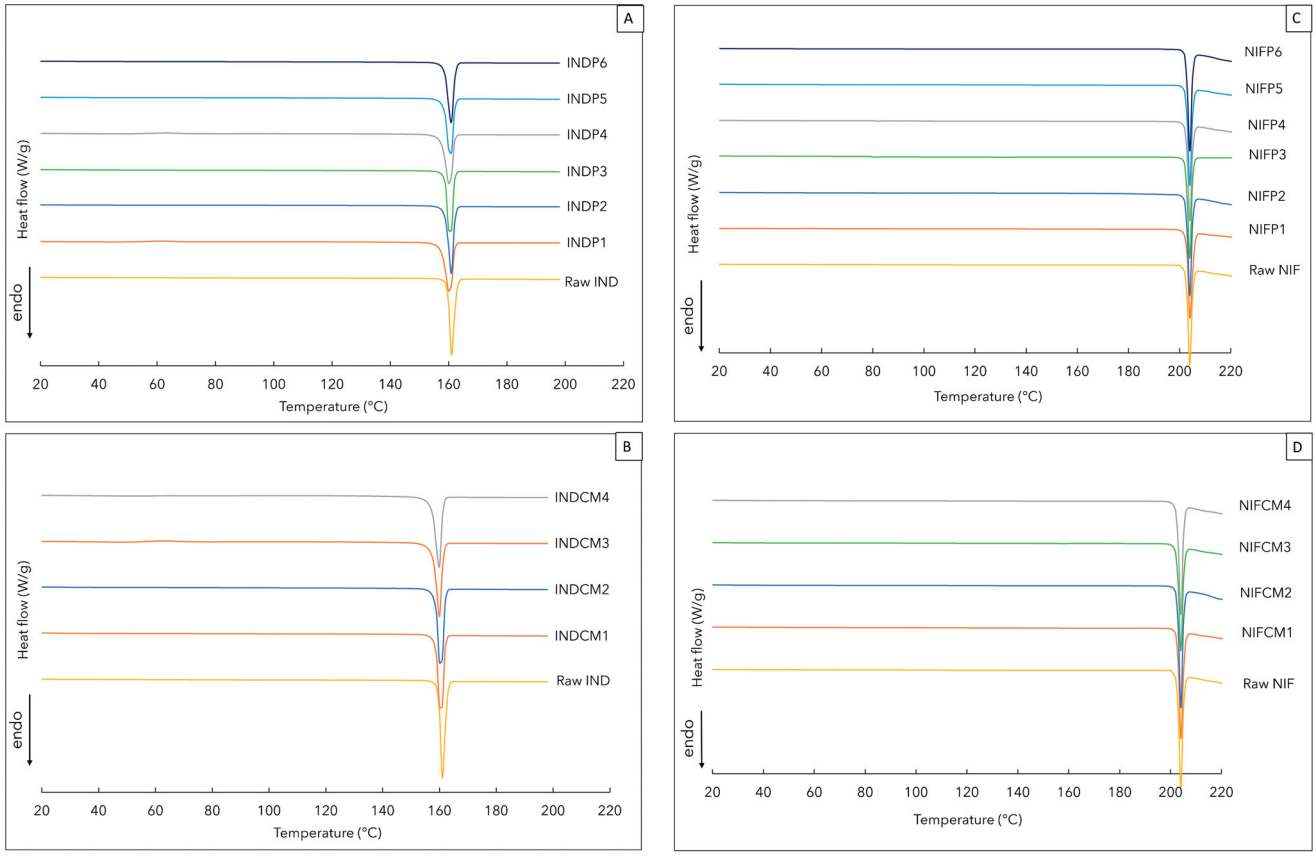

Figure 4. DSC thermograms. (A) IND ground with Pulverisette 0®, (B) IND ground with CryoMill®, (C) NIF ground with Pulverisette 0®, and (D) NIF ground with CryoMill®.

Table 5. Thermal properties.

	IND					NIF				
Milling equipment	Sample name	$T_{m(onset)}$ (°C)	T_m (°C)	ΔH_F (J/g)	Residual crystallinity (%)	Sample name	$T_{m(onset)}$ (°C)	T_m (°C)	ΔH_F (J/g)	Residual crystallinity (%)
	Raw IND	159.8	160.9	111	100	Raw NIF	203.0	203.8	128.7	100
P0	INDP1	**158.0**	**160.2**	**106.1**	**96**	NIFP1	202.9	203.8	128.2	100
	INDP2	159.4	160.5	107.6	97	NIFP2	203.0	203.7	129.0	100
	INDP3	159.5	160.5	109.2	98	NIFP3	202.9	203.6	131.4	102
	INDP4	**158.0**	**160.3**	**104.3**	**94**	NIFP4	203.0	203.8	130.9	102
	INDP5	159.1	160.4	107.8	97	NIFP5	202.9	203.7	130.3	101
	INDP6	159.5	160.5	108.9	98	NIFP6	202.9	203.7	129.5	101
CM	INDCM1	159.4	160.5	109.2	98	NIFCM1	203.0	203.8	129.6	101
	INDCM2	159.1	160.4	107.4	97	NIFCM2	202.9	203.8	128.2	100
	INDCM3	**157.9**	**160.1**	**105.7**	**95**	NIFCM3	202.8	203.7	128.9	100
	INDCM4	**157.6**	**160.0**	**104.2**	**94**	NIFCM4	202.9	203.9	128.2	100

be assigned to the C–Cl absorption bands. In addition, intense bands in the low frequency range, specific to aromatic compounds, are present between 760 and 980 cm^{-1}.

Pure NIF spectrum shows characteristics peaks (see Figure 5(C,D)) at 1662 cm^{-1} (C= O stretching vibrations), 1140–1170 cm^{-1} (C–F stretching vibrations) and also intensive bands at 760 and 980 cm^{-1} related to aromatic compounds (Saravanan et al. 2021).

For both APIs, similar FTIR spectra were noticed for processed and unprocessed powders suggesting no changes between the internal structure and conformation of these samples (Sheng et al. 2006; Serajuddin 2007; Sud and Kamath 2013). Nevertheless, minor differences can be observed on peaks intensity of the bands, which can be associated to method reproducibility linked to the contact area between the sample and the ATR crystal (Szunyogh et al. 2012).

3.3.2. Dynamic vapor sorption

At early pharmaceutical development, it is essential to know the hygroscopic nature of an API for a better understanding of its physicochemical behavior. Figure 6(A,B), with DVS results for raw IND and NIF showed non-hygroscopic solids at 95% RH, which exhibited low moisture absorption, <1% for IND and 0% for NIF over specified humidity range.

After grinding for both APIs, an increase of moisture absorption is observed with DVS (absorptions and desorption) profiles. For IND, humidity uptake was increased from 2- up to 5-fold. For NIF, a slight increase of 0.04% was observed. In addition, an overlap of water uptake curves is observed. This behavior can indicate that ground powders are stable crystalline solids and that crystal internal structure is not affected by high RH% (Szunyogh et al. 2013).

According to samples INDP1, INDP4, INDCM3, and INDCM4 isotherms, it was noted that the water uptake for these sample is

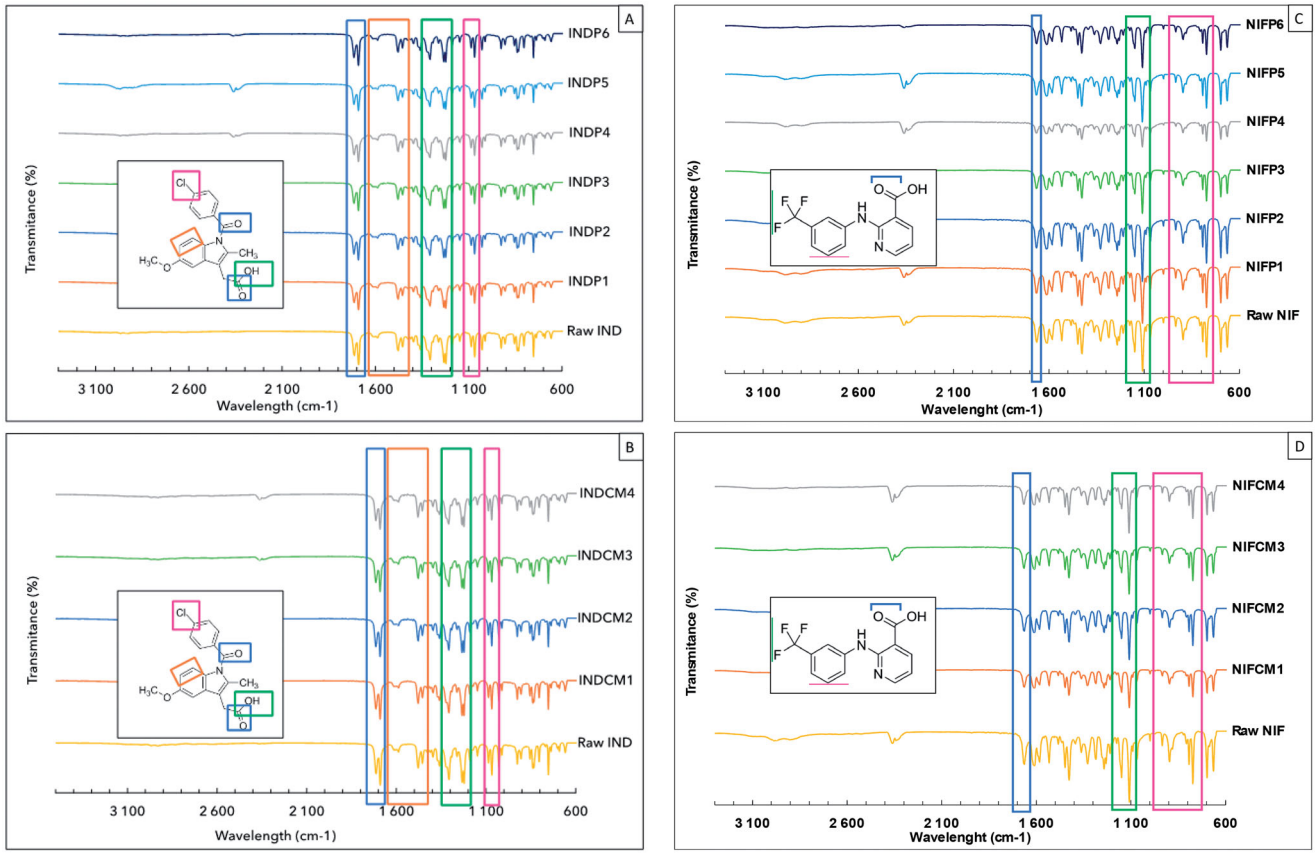

Figure 5. FTIR spectra. (A) IND ground with Pulverisette 0®, (B) IND ground with CryoMill®, (C) NIF ground with Pulverisette 0®, and (D) NIF ground with CryoMill®.

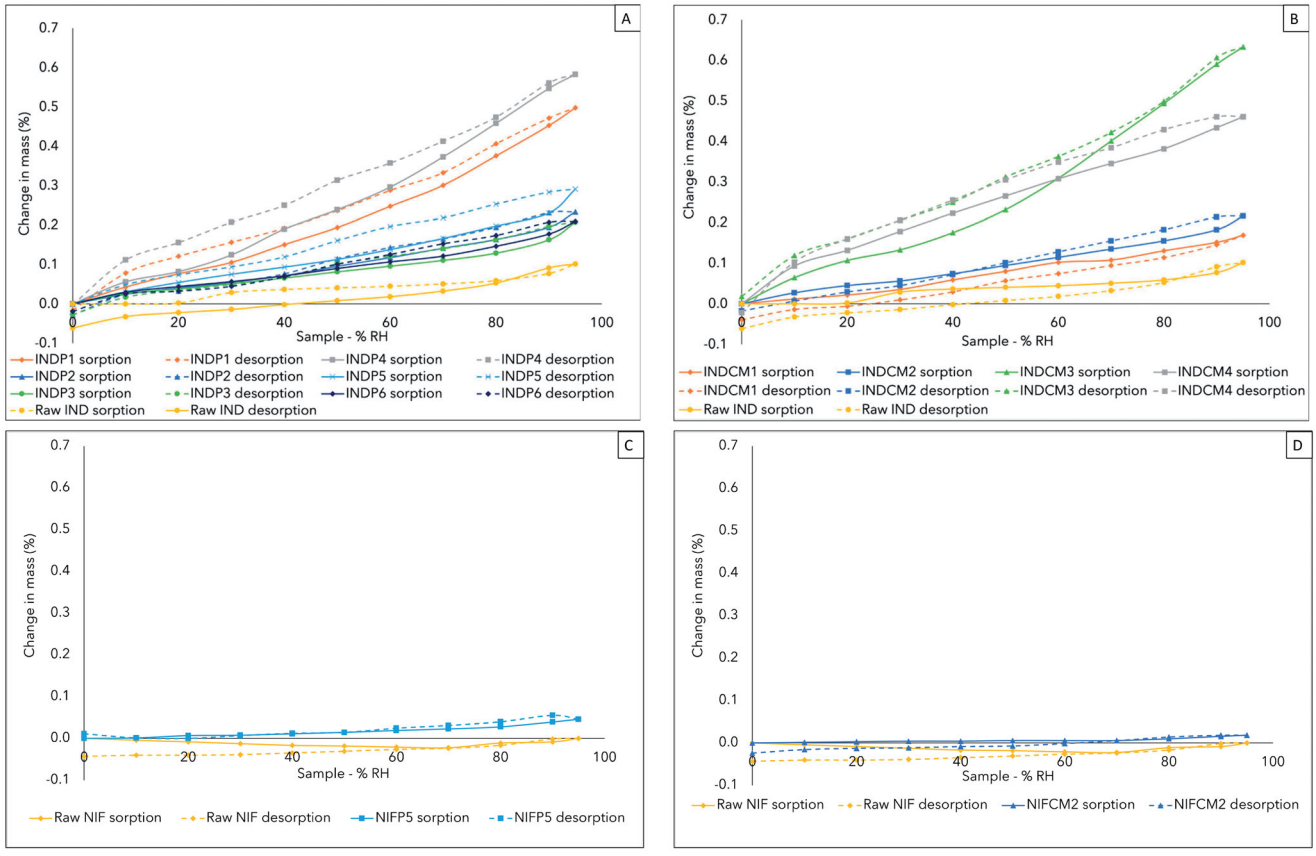

Figure 6. DVS isotherm plot. (A) IND ground with Pulverisette 0®, (B) IND ground with CryoMill®, (C) NIF ground with Pulverisette 0®, and (D) NIF ground with CryoMill®.

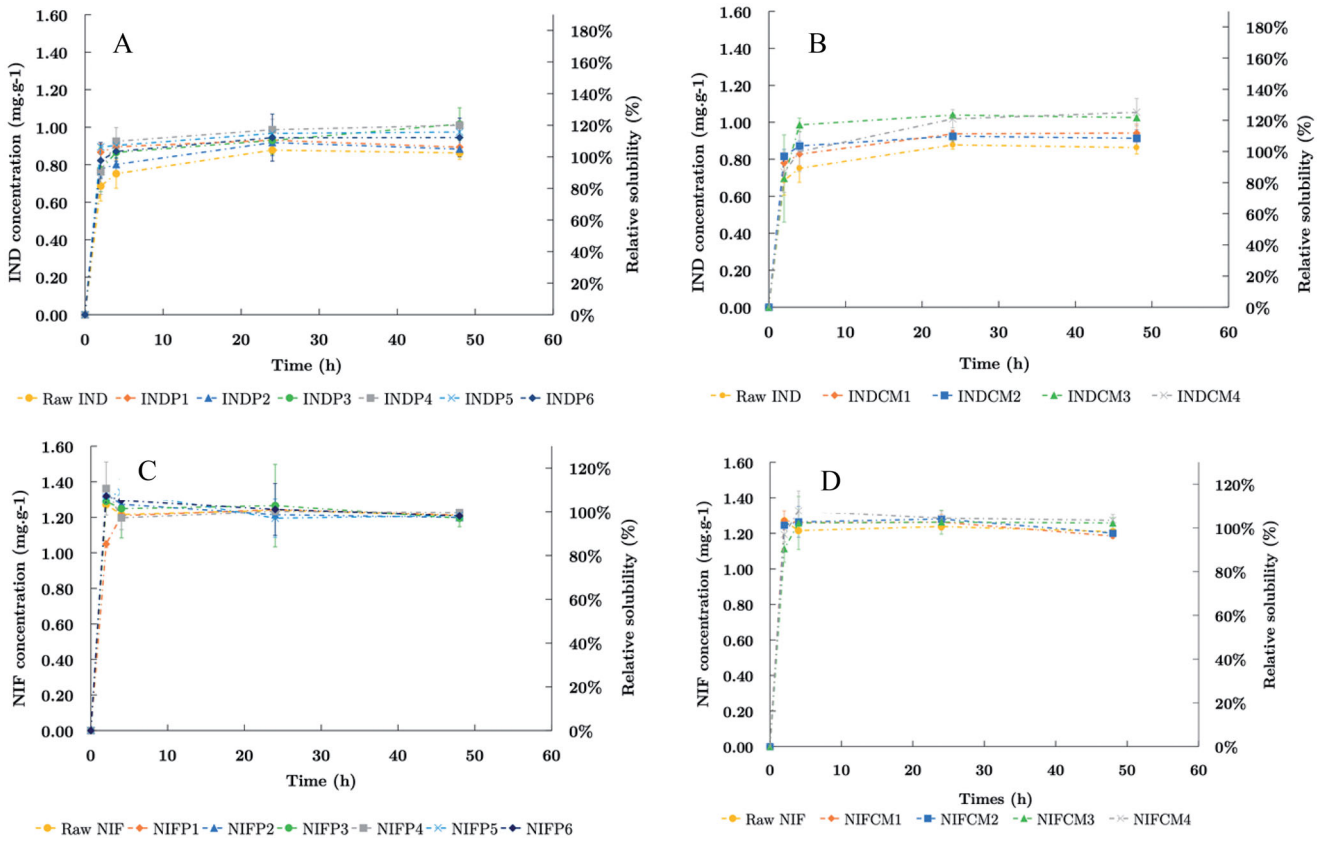

Figure 7. Solubility kinetics profiles at 37 °C in aqueous media at different time points (2 h, 4 h, 24 h, and 48 h). (A) IND ground with Pulverisette 0®, (B) IND ground with CryoMill®, (C) NIF ground with Pulverisette 0®, and (D) NIF ground with CryoMill®. Values are displayed as mean with standard deviation ($n = 4$).

Table 6. Equilibrium concentration values at 2 h, 4 h, and 24 h of IND and NIF.

	IND				NIF			
Milling equipment	Sample name	C_{IND} at 2 h (mg.g^{-1})	C_{IND} at 4 h (mg.g^{1})	C_{eq} at 24 h (mg.g^{-1})	Sample name	C_{NIF} at 2 h (mg.g^{-1})	C_{NIF} at 4 h (mg.g^{-1})	C_{eq} at 24 h (mg.g^{-1})
–	Raw IND	0.68 ± 0.08	0.75 ± 0.08	0.75 ± 0.08	Raw NIF	1.27 ± 0.01	1.22 ± 0.01	1.21 ± 0.01
P0	INDP1	0.87 ± 0.04	0.90 ± 0.05	0.90 ± 0.05	NIFP1	1.05 ± 0.02	1.21 ± 0.03	1.21 ± 0.01
	INDP2	0.78 ± 0.12	0.80 ± 0.03	0.80 ± 0.03	NIFP2	1.33 ± 0.01	1.27 ± 0.02	1.22 ± 0.02
	INDP3	0.77 ± 0.12	0.87 ± 0.03	0.87 ± 0.03	NIFP3	1.29 ± 0.01	1.25 ± 0.16	1.20 ± 0.23
	INDP4	0.76 ± 0.12	0. 92 ± 0.07	0.92 ± 0.07	NIFP4	1.36 ± 0.15	1.20 ± 0.07	1.23 ± 0.04
	INDP5	0.89 ± 0.01	0.90 ± 0.01	0.90 ± 0.01	NIFP5	1.32 ± 0.01	1.34 ± 0.01	1.21 ± 0.15
	INDP6	0.82 ± 0.01	0.87 ± 0.05	0.87 ± 0.05	NIFP6	1.32 ± 0.01	1.30 ± 0.01	1.20 ± 0.15
CM	INDCM1	0.78 ± 0.25	0.83 ± 0.06	0.83 ± 0.06	NIFCM1	1.27 ± 0.05	1.26 ± 0.01	1.19 ± 0.04
	INDCM2	0.82 ± 0.04	0.87 ± 0.03	0.87 ± 0.03	NIFCM2	1.25 ± 0.01	1.27 ± 0.09	1.20 ± 0.01
	INDCM3	0.70 ± 0.24	0.99 ± 0.04	0.99 ± 0.04	NIFCM3	1.11 ± 0.08	1.26 ± 0.15	1.26 ± 0.07
	INDCM4	0.73 ± 0.11	0.84 ± 0.11	0.84 ± 0.11	NIFCM4	1.19 ± 0.04	1.33 ± 0.11	1.28 ± 0.04

Values are displayed as mean with standard deviation ($n = 4$).

higher. As reported by Saleki-Gerhardt, this behavior can denote crystallinity loss by amorphous regions or formation of crystal defects after grinding (Taniguchi et al. 2014). The DVS measurements were also carried out for raw NIF as well as for the ground samples in a lower number of samples which are representative of API comportment at high RH%. As shown in Figure 6(C,D), it appears that NIF, despite the grinding, continued to present an important non-hygroscopic behavior.

3.4. Milling influence on drug solubility and dissolution kinetics

IND and NIF are considered as poorly soluble in aqueous media. The solubilization process was followed at 2 h, 4 h, 24 h, and 48 h, until APIs equilibrium concentration is reached. According to Figure 7, all milled IND samples showed faster solubilization kinetics compared to the raw material. It would appear that the INDP1, INDCM3, and INDCM4 samples have a faster solubilization rate with a maximum value at 4 h for the INDCM3 concentration C_{IND} as 0.99 ± 0.04 mg.g^{-1}. In addition, no 'spring effect' was noticed, which can indicate a good API stability over the time (Tawfeek et al. 2020). Unlike milled NIF, any impact was observed on solubilization process as a function of the processes used and its different parameters.

In Table 6, the equilibrium concentration values at 24 h in aqueous buffer pH 7.2 at 37 °C are detailed. It can be noted that the equilibrium concentration reached for commercial IND is 0.75 ± 0.08 mg.g^{-1}, which is in accordance with previous work (Van Duong et al. 2018). Milled IND showed an increase, from 1.05- up to 1.2-folds on equilibrium concentration (see Table 6). Maximum solubility values observed were 0.92 ± 0.07 mg.g^{-1} for

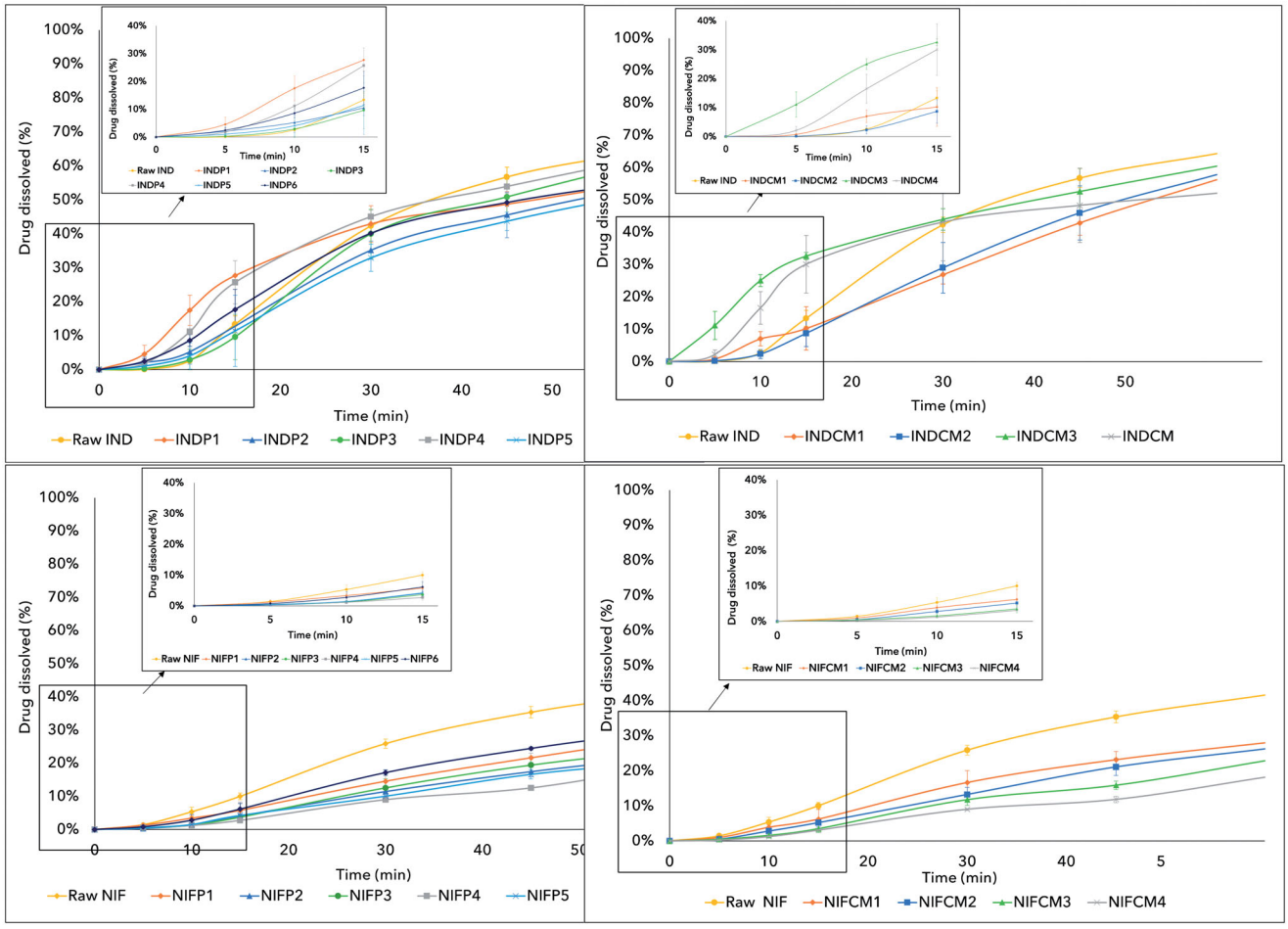

Figure 8. Dissolution profiles. (A) IND ground with Pulverisette 0®, (B) IND ground with CryoMill®, (C) NIF ground with Pulverisette 0®, and (D) NIF ground with CryoMill®. Values are displayed as mean with standard deviation ($n = 3$).

Table 7. Percentage of drug dissolved within the first 15 min.

	IND			NIF		
Milling equipment	Sample name	10 min (%)	15 min (%)	Sample name	10 min (%)	15 min (%)
–	Raw IND	2.6 ± 0.4	13.4 ± 2.5	Raw NIF	5.4 ± 1.4	10.1 ± 1.1
P0	INDP1	**17.5 ± 4.4**	**27.7 ± 0.2**	NIFP1	3.4 ± 1.9	5.8 ± 2.5
	INDP2	5.2 ± 3.5	10.5 ± 2.7	NIFP2	1.4 ± 0.4	4.1 ± 0.8
	INDP3	2.9 ± 3.1	9.7 ± 6.7	NIFP3	1.3 ± 0.2	3.7 ± 0.6
	INDP4	**11.2 ± 6.6**	**25.8 ± 6.1**	NIFP4	1.2 ± 0.4	2.8 ± 0.8
	INDP5	4.1 ± 3.8	11.4 ± 10.5	NIFP5	1.5 ± 0.1	4.24 ± 1.1
	INDP6	8.6 ± 1.7	17.7 ± 5.9	NIFP6	2.8 ± 1.8	6.2 ± 1.6
CM	INDCM1	7.0 ± 2.2	10.2 ± 6.7	NIFCM1	3.9 ± 0.7	6.2 ± 2.8
	INDCM2	2.3 ± 1.4	8.7 ± 4.1	NIFCM2	2.8 ± 0.6	5.2 ± 1.2
	INDCM3	**25.1 ± 1.8**	**32.6 ± 1.1**	NIFCM3	1.6 ± 0.6	3.5 ± 1.1
	INDCM4	**16.6 ± 5.1**	**30.1 ± 8.9**	NIFCM4	1.2 ± 0.1	3.1 ± 0.1

Values are displayed as mean with standard deviation ($n = 3$).

the INDP4, $0.99 \pm 0.04\ mg.g^{-1}$ and $0.84 \pm 0.11\ mg.g^{-1}$ for the INDCM3 and INDCM4 samples. As shown in Table 6, NIF equilibrium concentration does not change after milling compared to raw powder whether the samples are milled with the Pulverisette 0® or with the CryoMill®, for all samples the equilibrium solubility at pH 7.2 remains at approximately $1.21\ mg.g^{-1}$.

3.4.1. Dissolution kinetics evaluation

In vitro dissolution kinetics was carried out in pH 7.2 buffer, the dissolution profiles of the commercial molecules as well as the ground samples are shown in Figure 8. The dissolution testing shows an increase in the dissolution rate of ground IND compared to commercial drug in the first 10 min (see Table 7). These values indicate that there is a marked increase on dissolution rate from all ground IND samples mainly for INDP1, INDP4, INDCM3, and INDCM4 (see bold vaules-Table 7). The faster dissolution kinetics, at this stage, led to a maximum of 25% of DD against approximately 2% of DD for original drug. The increase of the dissolution rate can be attributed to the fine particles present for the 15 first minutes and its slowing down seems to be linked to the presence of powder agglomerates that were observed by SEM.

Dissolution study confirmed the enhancement of the initial dissolution rate of ground IND crystals by a decrease up to 40% of average particle size in number compared to the raw material and modification of surface properties (i.e. water vapor sorption, particle surface crystallinity) which can be potentially related to

increase of surface area and crystallinity change after drug milling, respectively. In addition, these results corroborate with DVS and with crystallinity evaluation which indicated the appearance of surface defaults, that potentially could enhance drug dissolution kinetics (Venkatesh et al. 1996). On the other hand, the dissolution kinetics of NIF, Figure 8(C,D) is not improved. The decrease of the dissolution initial rate of ground NIF crystals compared to raw material (see Table 7) was noticed. This behavior can be linked to the milling process, that primarily causes powder agglomeration and consequent reduction of surface area (Wadhwa et al. 2012).

4. Conclusions

The present study highlights that the use of the dry ball milling process could be an interesting way to improve the solubility and dissolution rate of BCS class II molecules. These processes are easy to implement and inexpensive. They avoid the use of organic solvents and are suitable for hydrophobic drugs to improve solubility and dissolution kinetics. The IND samples generated exhibit an improvement in solubility up to 1.2-fold and initial dissolution rates over the original product: a maximum of 25% of DD against 2% for original drug. Dry milling, whether with the Pulverisette 0® or the CryoMill®, leads to crystal surface modifications, where a decrease in crystallinity and an increase of the water sorption were observed: increase of humidity uptake from 2- up to 5-fold. In addition, no other physicochemical evolution was noticed. In contrast, for the NIF samples, any physicochemical modification or crystallinity decrease, that would allow an improvement in solubility or even dissolution kinetics, was noted. Both milling technologies seem not be suitable for NIF, because they lead to powder aggregate formation that would inhibit improvement in solubility properties and dissolution rate. These milling technologies would be interesting for pharmaceutical studies. However, additional investigation would be interesting to understand which type of crystal disorder governs the APIs physicochemical properties modification: amorphous regions or formation of crystal defects after grinding. This article gives a detailed and comprehensive description about the use of different dry milling processes for improving solubility, dissolution, and bioavailability of hydrophobic drugs. It highlighted that these properties improvement is not only linked to the process parameters, but mainly to the process and API synergy.

Acknowledgements

The authors are grateful to P. Accart, S. Del Confetto, V. Nallet, and S. Patry from Rapsodee Center for respectively analyses of particle size, DSC, XRD, and DVS.

Disclosure statement

The authors report no conflicts of interest. The authors alone are responsible for the content and writing of the paper.

Funding

The author(s) reported there is no funding associated with the work featured in this article.

References

Al-Obaidi H, Lawrence MJ, Shah S, Moghul H, Al-Saden N, Bari F. 2013. Effect of drug–polymer interactions on the aqueous solubility of milled solid dispersions. Int J Pharm. 446(1–2):100–105.

Amidon GL, Lennernäs H, Shah VP, Crison JR. 1995. A theoretical basis for a biopharmaceutic drug classification: the correlation of in vitro drug product dissolution and in vivo bioavailability. Pharm Res. 12(3):413–420.

Borba PAA, Pinotti M, de Campos CEM, Pezzini BR, Stulzer HK. 2016. Sodium alginate as a potential carrier in solid dispersion formulations to enhance dissolution rate and apparent water solubility of BCS II drugs. Carbohydr Polym. 137:350–359.

Branham ML, Moyo T, Govender T. 2012. Preparation and solid-state characterization of ball milled saquinavir mesylate for solubility enhancement. Eur J Pharm Biopharm. 80(1):194–202.

Chamarthy SP, Pinal R. 2008. The nature of crystal disorder in milled pharmaceutical materials. Colloids Surf A. 331(1–2): 68–75.

Chaudhari SP, Dugar RP. 2017. Application of surfactants in solid dispersion technology for improving solubility of poorly water soluble drugs. J Drug Delivery Sci Technol. 41:68–77.

Chaudhary A, Nagaich U, Gulati N, Sharma VK, Khosa RL. 2012. Enhancement of solubilization and bioavailability of poorly soluble drugs by physical and chemical modifications: a recent review. J Adv Pharm Educ Res. 2:32–67.

Chikhalia V, Forbes RT, Storey RA, Ticehurst M. 2006. The effect of crystal morphology and mill type on milling induced crystal disorder. Eur J Pharm Sci. 27(1):19–26.

Columbano A, Buckton G, Wikeley P. 2003. Characterisation of surface modified salbutamol sulphate-alkylpolyglycoside microparticles prepared by spray drying. Int J Pharm. 253(1–2):61–70.

Da Silva FLO, Marques MBDF, Kato KC, Carneiro G. 2020. Nanonization techniques to overcome poor water-solubility with drugs. Expert Opin Drug Discov. 15(7):853–864.

De Gusseme A, Neves C, Willart JF, Rameau A, Descamps M. 2008. Ordering and disordering of molecular solids upon mechanical milling: the case of fananserine. J Pharm Sci. 97(11):5000–5012.

de Paiva Lacerda S, Espitalier F, Hoffart V, Ré MI. 2015. Liquid antisolvent recrystallization to enhance dissolution of CRS 74, a new antiretroviral drug. Drug Dev Ind Pharm. 41(11):1910–1920.

Dedroog S, Huygens C, Van den Mooter G. 2019. Chemically identical but physically different: a comparison of spray drying, hot melt extrusion and cryo-milling for the formulation of high drug loaded amorphous solid dispersions of naproxen. Eur J Pharm Biopharm. 135:1–12.

Dujardin N, Willart JF, Dudognon E, Danède F, Descamps M. 2013. Mechanism of solid state amorphization of glucose upon milling. J Phys Chem B. 117(5):1437–1443.

Einfalt T, Planinšek O, Hrovat K. 2013. Methods of amorphization and investigation of the amorphous state. Acta Pharm. 63(3): 305–334.

El-Badry M, Fetih G, Fathy M. 2009. Improvement of solubility and dissolution rate of indomethacin by solid dispersions in gelucire 50/13 and PEG4000. Saudi Pharm J. 17(3):217–225.

Feng T, Pinal R, Carvajal MT. 2008. Process induced disorder in crystalline materials: differentiating defective crystals from the amorphous form of griseofulvin. J Pharm Sci. 97(8):3207–3221.

Fix I, Steffens K. 2004. Quantifying low amorphous or crystalline amounts of alpha-lactose-monohydrate using X-ray powder diffraction, near-infrared spectroscopy, and differential scanning calorimetry. Drug Dev Ind Pharm. 30(5):513–523.

Friedrich H, Nada A, Bodmeier R. 2005. Solid state and dissolution rate characterization of co-ground mixtures of nifedipine and hydrophilic carriers. Drug Dev Ind Pharm. 31(8):719–728.
Garg A, Singh S, Rao VU, Bindu K, Balasubramaniam J. 2009. Solid state interaction of raloxifene HCl with different hydrophilic carriers during co-grinding and its effect on dissolution rate. Drug Dev Ind Pharm. 35(4):455–470.
Gotor FJ, Achimovicova M, Real C, Balaz P. 2013. Influence of the milling parameters on the mechanical work intensity in planetary mills. Powder Technol. 233:1–7.
Guo Y, Shalaev E, Smith S. 2013. Physical stability of pharmaceutical formulations: solid-state characterization of amorphous dispersions. TrAC Trends Anal Chem. 49:137–144.
Hadjittofis E, Isbell MA, Karde V, Varghese S, Ghoroi C, Heng JYY. 2018. Influences of crystal anisotropy in pharmaceutical process development. Pharm Res. 35(5):100.
Hagbani TA, Nazzal S. 2017. Curcumin complexation with cyclodextrins by the autoclave process: method development and characterization of complex formation. Int J Pharm. 520(1–2): 173–180.
Han X, Ghoroi C, To D, Chen Y, Davé R. 2011. Simultaneous micronization and surface modification for improvement of flow and dissolution of drug particles. Int J Pharm. 415(1–2): 185–195.
Humayun HY, Shaarani MNNM, Warrior A, Abdullah B, Salam MA. 2016. The effect of co-solvent on the solubility of a sparingly soluble crystal of benzoic acid. Proc Eng. 148:1320–1325.
Hussain A, Smith G, Khan KA, Bukhari NI, Pedge NI, Ermolina I. 2018. Solubility and dissolution rate enhancement of ibuprofen by co-milling with polymeric excipients. Eur J Pharm Sci. 123: 395–403.
Jermain SV, Brough C, Williams RO. 2018. Amorphous solid dispersions and nanocrystal technologies for poorly water-soluble drug delivery – an update. Int J Pharm. 535(1–2):379–392.
Jójárt I, Sovány T, Pintye-Hódi K, Kása P. 2012. Study of the behaviour of magnesium stearate with different specific surface areas on the surface of particles during mixing. J Adhes Sci Technol. 26(24):2737–2744.
Junyaprasert VB, Morakul B. 2015. Nanocrystals for enhancement of oral bioavailability of poorly water-soluble drugs. Asian J Pharm Sci. 10(1):13–23.
Kacso I, Rus L, Pop M, Borodi G, Bratu I. 2012. Structural characterization of ambazone salt with niflumic acid. Spectroscopy. 27(1):49–58.
Kho HX, Bae S, Bae S, Kim B-W, Kim JS. 2014. Planetary ball mill process in aspect of milling energy. J Korean Powder Metall Inst. 21(2):155–164.
Kumar D, Worku ZA, Gao Y, Kamaraju VK, Glennon B, Babu RP, Healy AM. 2018. Comparison of wet milling and dry milling routes for ibuprofen pharmaceutical crystals and their impact on pharmaceutical and biopharmaceutical properties. Powder Technol. 330:228–238.
Kumar R, Thakur AK, Chaudhari P, Banerjee N. 2022. Particle size reduction techniques of pharmaceutical compounds for the enhancement of their dissolution rate and bioavailability. J Pharm Innov. 17(2):333–352.
Li J, Yang Y, Zhao M, Xu H, Ma J, Wang S. 2017. Improved oral bioavailability of probucol by dry media-milling. Mater Sci Eng C Mater Biol Appl. 78:780–786.
Ling Z, Wang T, Makarem M, Santiago Cintrón M, Cheng HN, Kang X, Bacher M, Potthast A, Rosenau T, King H, et al. 2019. Effects of ball milling on the structure of cotton cellulose. Cellulose. 26(1):305–328.
Loftsson T, Brewster ME. 2010. Pharmaceutical applications of cyclodextrins: basic science and product development. J Pharm Pharmacol. 62(11):1607–1621.
Loh ZH, Samanta AK, Heng PWS. 2015. Overview of milling techniques for improving the solubility of poorly water-soluble drugs. Asian J Pharm Sci. 10(4):255–274.
Mallick S, Pattnaik S, Swain K, De PK, Saha A, Ghoshal G, Mondal A. 2008. Formation of physically stable amorphous phase of ibuprofen by solid state milling with kaolin. Eur J Pharm Biopharm. 68(2):346–351.
Mallick S, Pradhan SK, Mohapatra R. 2013. Effects of microcrystalline cellulose based comilled powder on the compression and dissolution of ibuprofen. Int J Biol Macromol. 60:148–155.
Mártha C, Kürti L, Farkas G, Jójárt-Laczkovich O, Szalontai B, Glässer E, Deli MA, Szabó-Révész P. 2013. Effects of polymers on the crystallinity of nanonized meloxicam during a co-grinding process. Eur Polym J. 49(9):2426–2432.
Mennini N, Maestrelli F, Cirri M, Mura P. 2016. Analysis of physicochemical properties of ternary systems of oxaprozin with randomly methylated-β-cyclodextrin and L-arginine aimed to improve the drug solubility. J Pharm Biomed Anal. 129: 350–358.
Mir M, Hayat K, Hussain T, Waqas MK, Bukhari NI. 2018. Ball mill based on co-milling, a promising way to enhance solubility of poorly soluble drugs employing norfloxacin as model drug. Acta Pol Pharm. 75(1):155–168.
Newman A, Zografi G. 2014. Critical considerations for the qualitative and quantitative determination of process-induced disorder in crystalline solids. J Pharm Sci. 103(9):2595–2604.
Noyes AA, Whitney WR. 1897. The rate of solution of solid substances in their own solutions. J Am Chem Soc. 19(12):930–934.
Nugrahani I, Jessica MA. 2021. Amino acids as the potential co-former for co-crystal development: a review. Molecules. 26(11): 3279.
Patterson JE, James MB, Forster AH, Lancaster RW, Butler JM, Rades T. 2007. Preparation of glass solutions of three poorly water soluble drugs by spray drying, melt extrusion and ball milling. Int J Pharm. 336(1):22–34.
Perissutti B, Passerini N, Trastullo R, Keiser J, Zanolla D, Zingone G, Voinovich D, Albertini B. 2017. An explorative analysis of process and formulation variables affecting comilling in a vibrational mill: the case of praziquantel. Int J Pharm. 533(2): 402–412.
Phillips EM. 1997. An approach to estimate the amorphous content of pharmaceutical powders using calorimetry with no calibration standards. Int J Pharm. 149(2):267–271.
Qin L, Niu Y, Wang Y, Chen X. 2018. Combination of phospholipid complex and submicron emulsion techniques for improving oral bioavailability and therapeutic efficacy of water-insoluble drug. Mol Pharm. 15(3):1238–1247.
Sakher E, Loudjani N, Benchiheub M, Bououdina M. 2018. Influence of milling time on structural and microstructural parameters of Ni_{50} Ti_{50} prepared by mechanical alloying using Rietveld analysis. J Nanomater. 2018:1–11.
Saleki-Gerhardt A, Ahlneck C, Zografi G. 1994. Assessment of disorder in crystalline solids. Int J Pharm. 101(3):237–247.
Saravanan D, Muthudoss P, Khullar P, Venis R. 2021. Micronization and agglomeration: understanding the impact of API particle properties on dissolution and permeability using solid state and biopharmaceutical "Toolbox". J Pharm Innov. 16(1): 136–151.
Serajuddin ATM. 2007. Salt formation to improve drug solubility. Adv Drug Deliv Rev. 59(7):603–616.

Sheng JJ, Kasim NA, Chandrasekharan R, Amidon GL. 2006. Solubilization and dissolution of insoluble weak acid, ketoprofen: effects of pH combined with surfactant. Eur J Pharm Sci. 29(3–4):306–314.

Sud S, Kamath A. 2013. Methods of size reduction and factors affecting size reduction in pharmaceutics. Int Res J Pharm. 4(8): 57–64.

Szunyogh T, Ambrus R, Szabó-Révész P. 2012. Formation of niflumic acid particle size by solvent diffusion and solvent evaporation as precipitation methods. J Drug Delivery Sci Technol. 22(4):307–312.

Szunyogh T, Ambrus R, Szabó-Révész P. 2013. Nanonization of niflumic acid by co-grinding. Adv Nanopart. 2(4):329–335.

Taniguchi C, Kawabata Y, Wada K, Yamada S, Onoue S. 2014. Microenvironmental pH-modification to improve dissolution behavior and oral absorption for drugs with pH-dependent solubility. Expert Opin Drug Deliv. 11(4):505–516.

Tawfeek HM, Chavan T, Kunda NK. 2020. Effect of spray drying on amorphization of indomethacin nicotinamide cocrystals; optimization, characterization, and stability study. AAPS PharmSciTech. 21:181.

Van Duong T, Lüdeker D, Van Bockstal P-J, De Beer T, Van Humbeeck J, Van den Mooter G. 2018. Polymorphism of indomethacin in semicrystalline dispersions: formation, transformation, and segregation. Mol Pharm. 15(3):1037–1051.

Venkatesh S, Li J, Xu Y, Vishnuvajjala R, Anderson BD. 1996. Intrinsic solubility estimation and pH-solubility behavior of cosalane NSC 658586, an extremely hydrophobic diprotic acid. Pharm Res. 13(10):1453–1459.

Wadhwa J, Nair A, Kumria R. 2012. Emulsion forming drug delivery system for lipophilic drugs. Acta Pol Pharm. 69:179–191.